Electronic Supplementary Information (ESI)

Trehalose-functional glycopeptide enhances glycerol-free cryopreservation of red blood cells

Bo Liu, Qifa Zhang, Yunhui Zhao, Lixia Ren and Xiaoyan Yuan*

School of Materials Science and Engineering, and Tianjin Key Laboratory of Composite and Functional Materials, Tianjin University, Tianjin 300350, China

E-mail: yuanxy@tju.edu.cn

Experimental Methods

Materials

ε-Polylysine (ε-**PL**, average molecular weight: ~4000) was purchased from Nanjing Xuankai Biotechnology, China. N_{α}-(tert- butyloxycarboryl)-N_{ω}-(4-toluenesulfonyl)-$_{L}$-arginine (Boc-Arg(Tos)-OH, **R**) was provided by Shanghai Bide Pharmatech, China. Fluorescein isothiocyanate (FITC), 1-ethyl-3-(3-dimethylaminopropyl) carbodiimide hydrochloride (EDCI), *N*-hydroxysuccinimide (NHS), triethylamine and succinic anhydride were provided by Tianjin Heowns Biochemical Technology, China. Sterile defibrinated sheep red blood cells (RBCs) were provided by Guangzhou Future Biotechnology, China. Anhydrous trehalose (**Tre**) and trifluoroacetic acid (TFA) were obtained from J&K Scientific Ltd., China. Sodium hydroxide, 3-(4,5-dimethlthiazol-2-yl)-2,5-diphenyltetrazoliumbromide (MTT), anhydrous dimethyl sulfoxide (DMSO), *N,N'*-dimethylformamide (DMF) and other solvents were supplied by Kermel Chemical Technology, China. 1,2-Dioleoyl-sn-glycero-3-phosphocholine (DOPC), *n*-octyl-β-$_{D}$-glucopyranoside, deuterium dimethyl sulfoxide (DMSO-d^6) and deuterium oxide (D_2O) were purchased from Sigma Aldrich (Energy Chemical, China). Dulbecco's modified eagle medium (DMEM) and fetal bovine serum certified (FBS) were purchased from Gibco. Alamar blue cell viability reagent was provided by Shanghai BestBio Biotechnology, China. All chemicals were used directly as received without further purification unless mentioned.

Synthesis of carboxylated trehalose

As illustrated in Scheme S1, carboxylated trehalose (**Tre-COOH**) was prepared by **Tre** reacting with succinic anhydride adopted from the reference.[1] **Tre** (3.5 g, 10.23 mmol) was dissolved in dry dimethylformamide (DMF, 100 mL), and succinic anhydride (960 mg, 9.6 mmol) was dissolved in dry DMF (20 mL). Then, **Tre** solution was mixed with succinic anhydride solution, and 7% triethylamine DMF solution was added to the above mixtures.

The reaction was continued for 12 h at 80 ℃ under a nitrogen atmosphere. The product was precipitated using a diethyl ether/acetone mixture (70/30, *v*/*v*) for three times and dried in a vacuum oven at 50 ℃ for 12 h.

Synthesis of (glyco)peptides

As shown in Fig. 1A, trehalose-functional (glyco)peptides were prepared by sequent reactions of ε-**PL** with Boc-Arg(Tos)-OH (**R**) and carboxylated trehalose (**T**re-COOH), adopted from the reference.[2] Typically, Boc-Arg(Tos)-OH (3.32g, 7.75 mmol), EDCI (3.56 g, 18.57 mmol) and NHS (2.14 g, 18.59 mmol) were dissolved in DMSO (40 mL) and stirred at room temperature for 30 min. ε-**PL** (1.0 g, 0.25 mmol) dissolved in deionized water (10 mL) was added into the mixture solution and maintained at room temperature for 3 days. The mixture solution was dialyzed against deionized water for 3 days (cut off 2000 Dalton) and freeze-dried. The obtained white solid product was then dissolved in TFA and reacted at room temperature for 4 h. The reaction mixture was precipitated with diethyl ether and centrifugated. The crude product ε-PL-*g*-Arg(Tos) (**PLR$_8$**) was purified *via* dialysis in deionized water for 3 days (cut off 2000 Dalton) and freeze-dried. Then, **PLR$_8$** was further reacted with carboxylated trehalose to synthesize ε-PL-*g*-Arg(Tos)-*g*-Tre (**PLR$_8$T$_{13}$**) in the same way. The product was purified *via* dialysis (cut off 2000 Dalton) against deionized water for 3 days and lyophilized.

Characterization

The molecular weight of carboxylated trehalose was measured by high resolution mass spectrometry (HRMS, miorOTOF-QII, Bruker). Chemical structures of **PLR** and **PLRT**s were verified by analyses of ^{1}H nuclear magnetic resonance (NMR, Brucker AV 400 MHz, Germany). The ^{1}H NMR measurement was performed *via* dissolving 10 mg of the specimen in DMSO-d^6 or D_2O. The 2D ^{1}H-^{1}H nuclear Overhauser effect spectroscopy (NOESY) NMR measurement was performed *via* dissolving 50 mg of the specimen in D_2O. The molecular

weights of **PLT**, **PLR**s and **PLRT**s were calculated by the integral of **T** and **R** related signals. The molecular weight and polydispersity of (glyco)peptides were obtained using an aqueous gel permeation chromatography (GPC) system (Viscotek, UK) with poly(ethylene glycol) as the standard. The eluent was sodium acetate buffer solution (0.5 M of NaAc and 0.5 M of HAc, pH= 4.5) at a flow rate of 1.0 mL·min^{-1} at 30 °C. The Fourier transform infrared (FTIR) spectra were obtained in the range from 1800 to 1400 cm^{-1} in PerkinElmer (Spectrum 100, USA) using the KBr pellet technique. RBCs before and after treatment with the (glyco)peptide were also observed with a scanning electron microscope (SEM, Hitachi su1510, Japan). The washed RBCs in 50 μL were added to 1 mL (glyco)peptide solution (0.1 mg·mL^{-1}). After being incubated at 37 °C for 2 h, the RBCs suspensions were dropped onto the slide, followed by fixation with 2.5% glutaraldehyde in PBS overnight. The fixed RBCs were dehydrated with a series of graded ethanol solutions (30, 50, 60, 70, 80 90, 95 and 100%, 15 min each), and then dried in air. The samples were gold-coated prior to being viewed by SEM. The circular dichroism (CD) spectra of (glyco)peptides were obtained using a CD spectrometer (J-810, Jasco, Japan) at room temperature under a constant flow of N_2. The polymer aqueous solutions (0.1 mg·mL^{-1}) were introduced into quartz cuvettes with a path length of 1 mm. The wavelengths were set at 185~250 nm with a scan speed of 100 nm·min^{-1}. The integration time was set at 1 second and the bandwidth was set to 0.5 nm. The water was used as the reference. All (glyco)peptide solutions were previously filtered using 0.22 μm filter and each sample was measured in triplicate.

Hemolysis assay

Sterile defibrinated sheep RBCs were used as cell model for evaluation hemolysis of synthesized (glyco)peptide.[3] RBCs washed with single strength PBS solution (306 mOsm, pH 7.4) for three times (centrifugation, 2000 rpm, 10 min, 4 ºC). Then, RBCs were resuspended in (glyco)peptide or (glyco)peptide/**Tre** buffer solutions. After being incubated at 37 ºC for 2

h, the optical density (OD) values of released hemoglobin were measured at 541 nm using a microplate reader (TECAN, Switzerland). The sample of RBCs in PBS buffer was taken as the negative control, and the sample of RBCs lysed with deionized water was used as the positive control. The relative hemolysis of each sample was calculated according to the following equation (S1).

$$\text{Relative hemolysis (\%)} = \frac{OD_{Sample} - OD_{Negative\ control}}{OD_{Positive\ control} - OD_{Negative\ control}} \times 100 \quad \text{(S1)}$$

Cytotoxicity

The cytotoxicity of the (glyco)peptide was examined by using L929 fibroblasts *via* Alamar Blue assay and MTT assay.[4-6] Firstly, cells were cultured in DMEM containing 10% FBS and 1% penicillin-streptomycin in a humidified incubator with 5% CO_2 at 37 ºC for 24 h. L929 cells were seeded into a 96-well plate (Corning) containing medium (0.2 mL per well) at a density of 1×10^4 cells per well for 24 h, respectively. The medium was replaced with 0.2 mL of DMEM containing 10% FBS and **PL**, **PLT**, **PLR** or **PLRT**s at specific concentrations, and the cells were cultured for another 24 h. The cytotoxicity was determined by MTT assay. For Alamar Blue assay, the cultural medium of 96-well plate containing L929 cells was replaced with the fresh culture composed of 10% Alamar Blue reagent after 24 h of incubation. Further incubated for 4 h was conducted according to the manufacturer's instruction, and the fluorescence of each well was measured using a microplate reader at excitation wavelength of 525 nm and emission wavelength of 590 nm. The relative cell viability was calculated as following equation (S2). For MTT assay, the cultural medium of 96-well plate containing L929 cells was replaced with 90 μL of fresh culture and 10 μL of MTT solution (5 $mg\cdot mL^{-1}$ in PBS) after being incubated for 24 h and cultured another 4 h. Subsequently, the liquid was removed, and 200 μL of DMSO were added and shocked at 100 rpm for 30 min to dissolve the blue crystal per well. The OD value was measured at 490 nm using the microplate reader.

The relative cell viability was calculated as following equation (S3). During the measurement, the medium without polymer was as the positive control, and each sample was repeated in triplicate.

$$\text{Relative cell viability (\%)} = \frac{I_{590,\text{ Sample}}}{I_{590,\text{ Positive control}}} \times 100 \quad \text{(S2)}$$

$$\text{Relative cell viability (\%)} = \frac{\text{OD}_{490,\text{ Sample}}}{\text{OD}_{490,\text{ Positive control}}} \times 100 \quad \text{(S3)}$$

LF ^{1}H NMR spectroscopy

The LF NMR spectra were obtained through a Bruker Minispec mq20 spectrometer operating at a proton resonance frequency of 20 MHz at ambient temperature according reference.[7-9] Samples were placed in the NMR tube with a 10 mm outer diameter. The free induction decay signals were recorded with Carr-Purcell-Meiboom-Gill (CPMG) pulse sequences, where the transverse spin-spin relaxation time (T_2) distribution curve was obtained through an inverse Laplace transform-based CONTIN analysis on the CPMG decay curves. Each sample was run with 4 scans and a 2 s recycle delay.

DOPC liposome preparation

The preparation of DOPC liposomes was adopted from the reference[10,11] DOPC was suspended in the HBS-N running buffer (10 mM HEPES, pH 7.4, 150 mM NaCl, Nanjing SenBeiJia Biological Technology Co., Ltd., China) and then treated through froze-thaw-vortex for 5 times to completely agitate it. The obtained DOPC suspension (10 mM) was stirred ultrasonically for 20 min using an ultrasonic cell disruptor (Scientz-IID, JY92-IIN) and the nanoscale liposomes were formed.

Surface plasmon resonance (SPR) spectroscopy

SPR spectroscopy analysis was used for characterizing of the interaction of glycopeptide or

Tre with a cell membrane model.[12,13] The L1 sensor chip was placed in the Biacore 3000 system (GE Healthcare) and washed with 40 mM *n*-octyl-β-$_D$-glucopyranoside at the flow rate of 10 μL·min^{-1} for 10 min. The 0.5 mM DOPC liposome, which was diluted in the HBS-N running buffer, was added to the sensor chip at a flow rate of 2 μL·min^{-1} to generate a lipid bilayer on the chip until achieving the resonance unit (RU) value at 6400. Then, the surface of the sensor chip was washed with 50 mM NaOH at 2 μL·min^{-1} for 5 min, and 100 μg·mL^{-1} BSA flowed over the sensor chip at 2 μL·min^{-1}. It was regarded that the stabilization of the liposome onto the sensor chip was achieved when the increased extent by the addition of BSA (RU values) was <100. The HBS-N buffer solutions were prepared containing (glyco)peptide or **Tre**. Sample solution was injected into the Biacore 3000 system at the flow rate of 10 μL·min^{-1} for 10 min, and then the running buffer was eluted. The SPR data were obtained using BIA evaluation software.

Differential scanning calorimetry (DSC) analysis

The energetics of the interactions between (glyco)peptide and DOPC were measured using a differential scanning calorimeter (PerkinElmer Diamond).[14-16] DSC assessment of ice formation was performed.[14,17] Samples were added to 40 μL aluminum pans and transferred to a Freon IntraCooler 2P cooling accessory (Heat flow, W·g^{-1}). The measurement was recorded against an empty pre-weighted 40 μL aluminum reference pan from 25 °C to -40 °C at 10 °C·min^{-1}, followed by -40 °C to 25 °C at 2 °C·min^{-1}, with the presence of two large endothermic peaks which demonstrated water freezing and ice melting.

Raman spectroscopy

Raman spectra were collected using a DXR Raman microscope with a 532 nm laser wavelength (Thermo Fisher Scientific Co. Ltd., USA).[8,15,18] The samples for the Raman spectra measurement were dropped into aluminum pans and placed the test bench to measure at a specified temperature. All samples were loaded on a temperature-controlled Linkam stage

(BCS196, UK) mounted on a Raman sample stage. The sample was cooled at a cooling rate of 2 ºC·min^{-1} from 20 ºC to -25 ºC and 10 ºC·min^{-1} from -25 ºC to -50 ºC. The samples were measured after being maintained at 20 ºC, 0 ºC, -25 ºC and -50 ºC for 5 min, respectively.

Cryopreservation protocol

Cryopreservation and evaluation of RBCs after post-thaw recovery were performed according to the references.[3,19] A 100 μL aliquot of RBCs was added to 1 mL (glyco)peptides or (glyco)peptides/**Tre** solutions in cryovials (Corning, 1.8 mL). RBCs were incubated at approximately 15% haematocrit (measured by BM 830, Beijing Baolingman Sunshine Technology Co., Ltd, China) in either 0.36 M **Tre** or 0.36 M **Tre**/1 mg·mL^{-1} (glyco)peptides for 7 h at 37 ºC and pH 7.4. Each sample was then directly plunged into liquid nitrogen immediately. For post-thaw recovery, cells were immediately thawed in a 37 ºC water bath. Post-thawed RBCs and control samples were centrifugated at 2000 rpm for 10 min, and the OD values of supernatant in each sample were measured at 541 nm using the microplate reader. The RBC cryosurvival was calculated in quadruplet samples by subtracting the hemolysis with the following equation (4).

$$\text{RBC cryosurvival (\%)} = (1 - \frac{\text{OD}_{\text{Sample}} - \text{OD}_{\text{Negative control}}}{\text{OD}_{\text{Positive control}} - \text{OD}_{\text{Negative control}}}) \times 100 \quad (4)$$

Confocal laser scanning microscopy

ε-**PL**, **PLR$_8$**, **PLT$_5$**, **PLR$_8$T$_{13}$** were reacted with fluoresceinisothiocyanate (FITC) at 0.01 molar ratio to polymer for 3 days at room temperature. FITC-polymer was purified by dialysis (Cut off 2000 Dalton) and freeze-dried.

RBCs (10^7 mL^{-1}) were resuspended and cultured at 37 ºC for 2 h in the buffer solution (pH = 7.4) in the presence of FTIC-polymers. Then, the RBCs mixtures were centrifuged at 3500 rpm for 3 minutes. When the supernatant was removed, the RBCs were resuspended in a 200 μL PBS solution. After RBCs being washed three times, the images of cells were recorded

using an inverted laser scanning confocal microscope (CLSM, Leica SP8, Germany) at the excitation wavelengths of 488 nm for FTIC-polymers.

Statistical analysis

All data points were repeated in triplicate. Results and graphical data are mean values with standard deviation encompassing a 95% confidence interval. Statistical analyses were performed using Student's *t*-test. A *p*-value less than 0.05 indicated statistically significant.

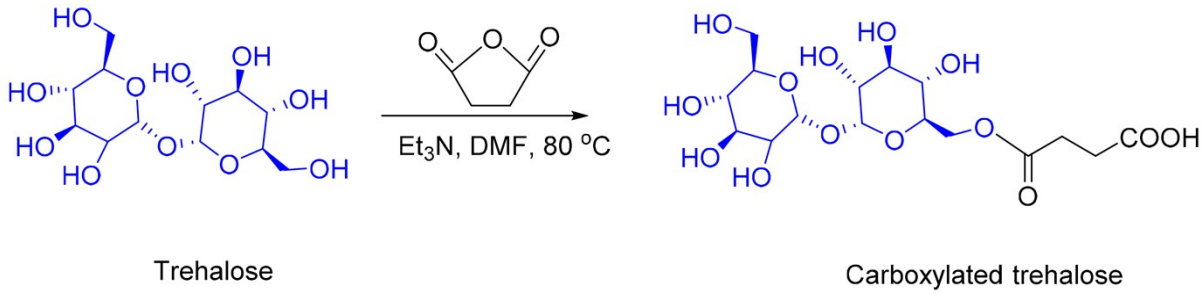

Trehalose

Carboxylated trehalose

Scheme S1 Synthesis of carboxylated trehalose.

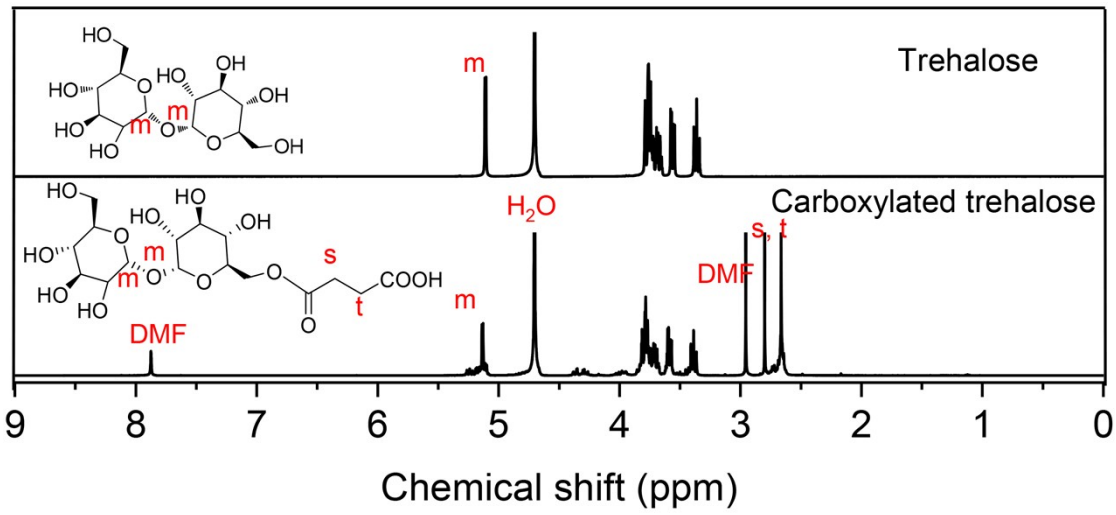

Fig. S1 ^{1}H NMR spectra of carboxylated trehalose.

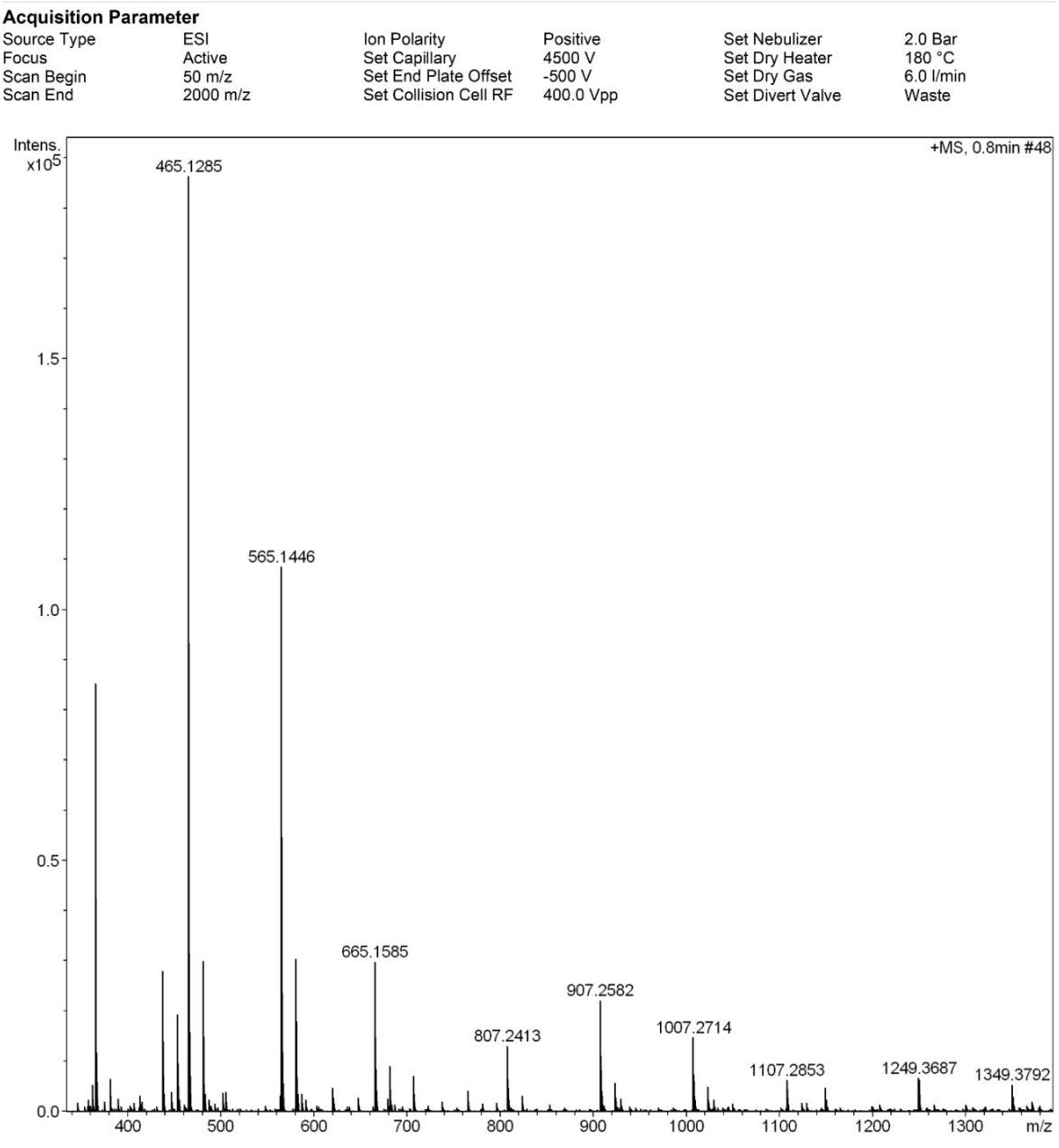

Fig. S2 HRMS spectrum of carboxylated trehalose.

Table S1 Percentage of trehalose, mono-carboxylated trehalose (Tre-$(COOH)_1$), di-carboxylated trehalose (Tre-$(COOH)_2$) and tri-carboxylated trehalose (Tre-$(COOH)_3$) calculated by HRMS spectrum.

Monomer	Formula	Calculated molecular weight [a)]	Detected molecular weight [b)]	m/z	Percentage (%)
Trehalose	$C_{12}H_{30}O_{11}$	350.30	350.02	350	20.7
Tre-$(COOH)_1$	$C_{16}H_{26}NaO_{14}$	465.36	465.13	465	45.1
Tre-$(COOH)_2$	$C_{20}H_{30}NaO_{17}$	565.43	565.15	565	26.8
Tre-$(COOH)_3$	$C_{24}H_{34}NaO_{20}$	665.51	665.16	665	7.4

[a)] Calculated results according the chemical formula of trehalose and its derivatives.

[b)] Detected results according to the HRMS spectrum.

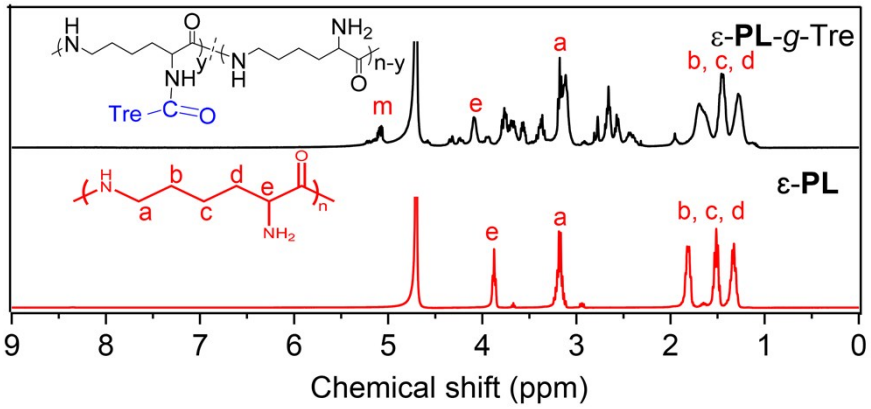

Fig. S3 ^{1}H NMR spectra of ε-PL-*g*-Tre (**PLT**).

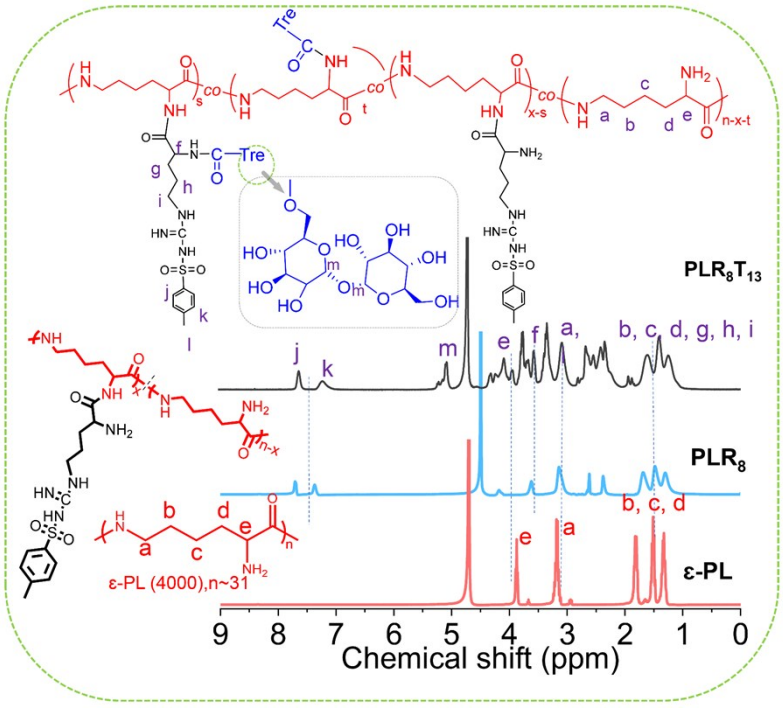

Fig. S4 ^{1}H NMR spectra of ε-**PL** and **Tre**-functional (glyco)peptides, **PLR$_8$** and **PLR$_8$T$_{13}$**. ε-**PL**, **PLR$_8$** and **PLR$_8$T$_{13}$** exhibited similar signal at δ 1~2 ppm, 3.0~3.5 ppm and 3.8~4.0 ppm in the ^{1}H NMR spectra, attributed to -C$\boldsymbol{H}_2$- and -C$\boldsymbol{H}$- of the polymer backbone. The signal at approximately δ 7~8 ppm in the spectra of **PLR$_8$** was assigned to -C$\boldsymbol{H}_2$- of phenyl. **PLR$_8$T$_{13}$** exhibited similar signals at δ 7~8 ppm in the spectra, assigned to the phenyl groups. In additional, the signal at δ 4.8 ppm in the spectra of **PLR$_8$T$_{13}$** was attributed to -C$\boldsymbol{H}_2$- of **Tre** residues.

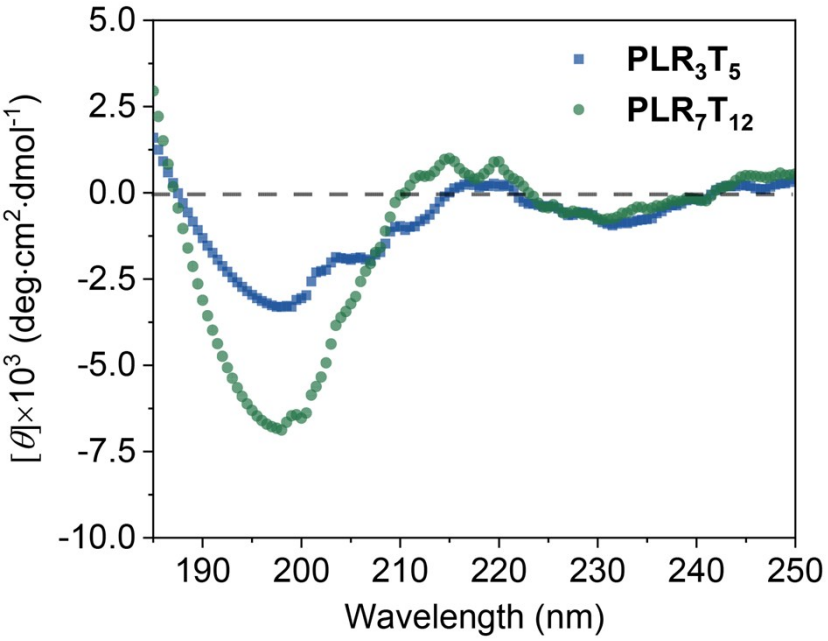

Fig. S5 CD spectra of **PLR_3T_5** and **PLR_7T_{12}** in aqueous solution at pH 7.4.

In Fig. S5, the CD spectrum of **PLR_3T_5** showed one negative band at 195~210 nm and one weak positive band at 215~220 nm. Similarly, the spectrum of **PLR_7T_{12}** showed one negative band at 195~205 nm and one weak positive band at 210~220 nm. The results indicated that the coexistence of the similar amphipathic polyproline II helix structure (negative signal) and random coils (weak positive signal), and the content of a similar amphipathic polyproline II helix structure for **PLR_7T_{12}** was higher than that of **PLR_3T_5**.

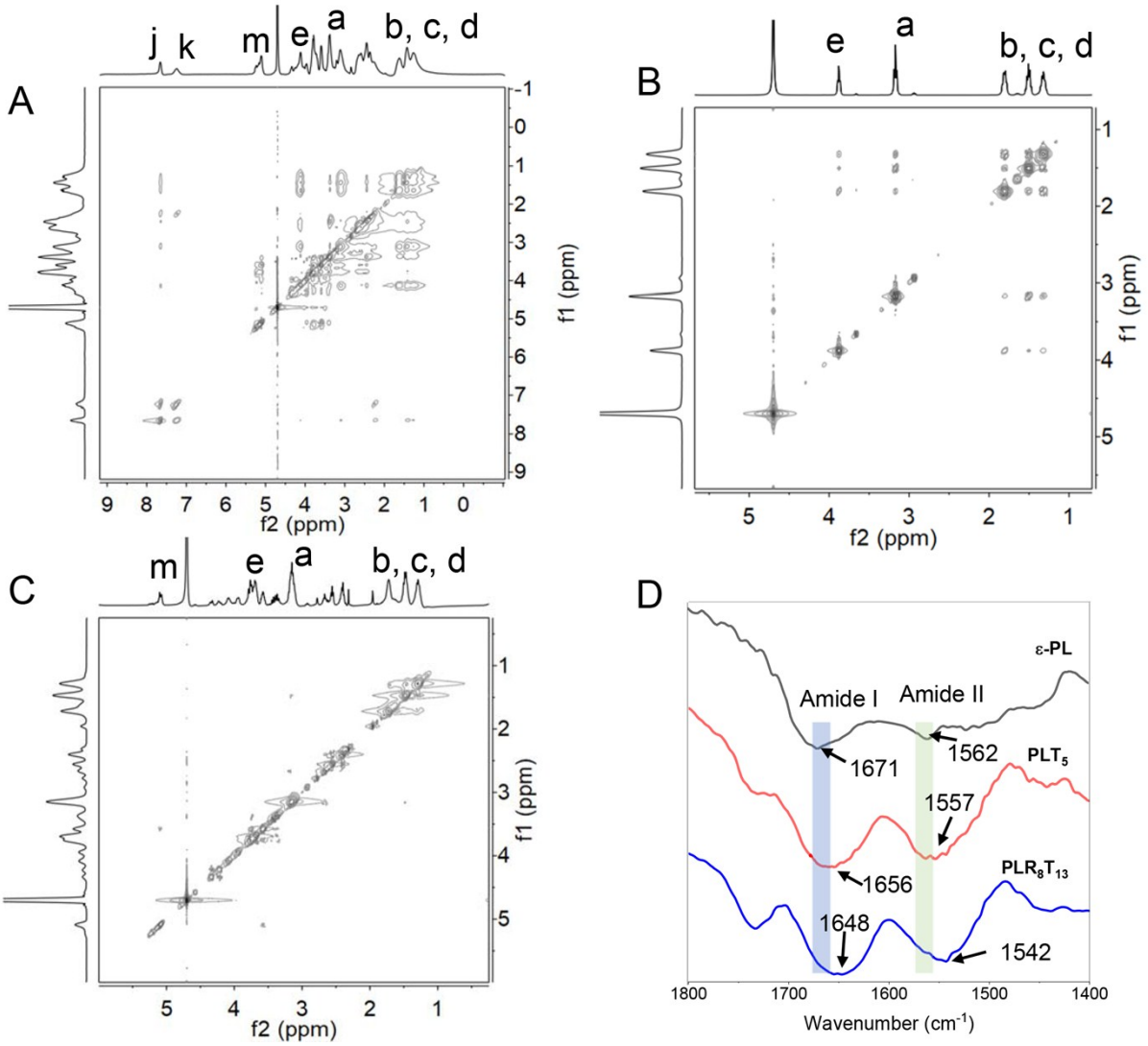

Fig. S6 2D ^{1}H-^{1}H NOESY spectra of (glyco)peptides in D_2O solutions. A) **PLR$_8$T$_{13}$**; B) ε-**PL**; C) **PLT$_5$**. D) FTIR spectra for selected fractions of (glyco)peptides in the amide I and amide II regions.

As shown in previous studies, NOESY spectra provided information about protons that was 5 Å or less apart in space, and the presence of a NOE peak (cross-peak) was the direct evidence that two protons are within 5 Å from each other in space.[20,21] As shown in Fig. S3 and Fig. S4, the chemical shifts of the hydrogen protons for **PLR$_8$T$_{13}$**, ε-**PL** and **PLT$_5$** have been discussed. Herein, Fig. S6A showed that hydrogen atoms bonded to carbon atoms (j, k, Arg(Tos)-C**H**, Fig. S4) produced NOE signals with hydrogen atoms in the backbone of ε-**PL** (a, b, c, d, e,

Lys-C**H$_2$**, Fig. S4). In addition, compared with NOESY spectrum of ε-**PL** (Fig. S6B), the intensities of cross-peaks were stronger among hydrogen atoms bond to carbon atoms with each other. The hydrogen atoms in the trehalose residue (m, Tre-C**H**, Fig. S4) also produced NOE signals with hydrogen atoms in the backbone of ε-**PL**. The results indicated that **PLR$_8$T$_{13}$** might exist in the folded state in aqueous solution. In contrast, no obvious signal NOE cross-peaks were found in **PLT$_5$** (Fig. S3 and Fig. S6C) between hydrogen atoms and other hydrogen atoms located farther away, indicating that the **PLT$_5$** might be extended in conformation.

FTIR spectra of proteins and polypeptides exhibited amide absorptions which represented different vibrations of the peptide moiety, such as amide I and amide II.[22-24] As shown in Fig. S6D, ε-**PL** displayed an amide I absorption peak at 1671 cm^{-1}, and it shifted to 1656 cm^{-1} (**PLT$_5$**) and 1648 cm^{-1} (**PLR$_8$T$_{13}$**), respectively. Meanwhile, the amide II absorption peak at 1562 cm^{-1} (**ε-PL**) shifted to 1557 cm^{-1} (**PLT$_5$**) and 1542cm^{-1} (**PLR$_8$T$_{13}$**), respectively. It was proposed that a conformation might change during amide I and amide II shifting.

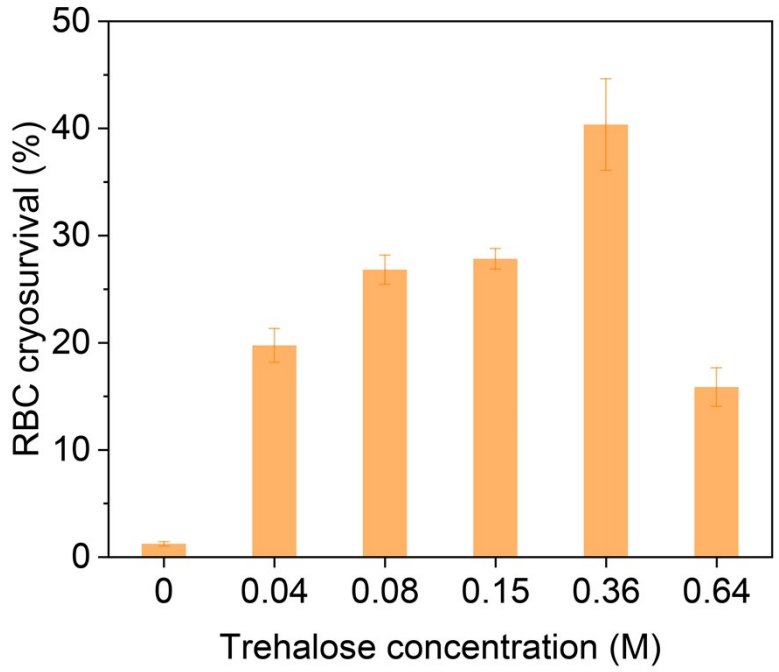

Fig. S7 RBC cryosurvival with different concentration of trehalose.

As shown in Fig. S7, the cryosurvival percentage of RBCs increased with concentration increase of **Tre** from 0 M to 0.36 M, and then the cryosurvival percentage of RBCs decreased when **Tre** concentration was 0.64 M. Although **Tre** could protect RBCs from cryoinjury during freezing and thawing, the higher concentration of **Tre** may cause significant increase of extracellular osmotic pressure from 300 mOsm to 600 mOsm (0.36 M **Tre**) or 1270 mOsm (0.64 M **Tre**), and then the RBCs could be damaged owing to severe dehydration.[25] Thus, in this study, the optimum **Tre** concentration was 0.36 M, similar to the results in the reference.[25]

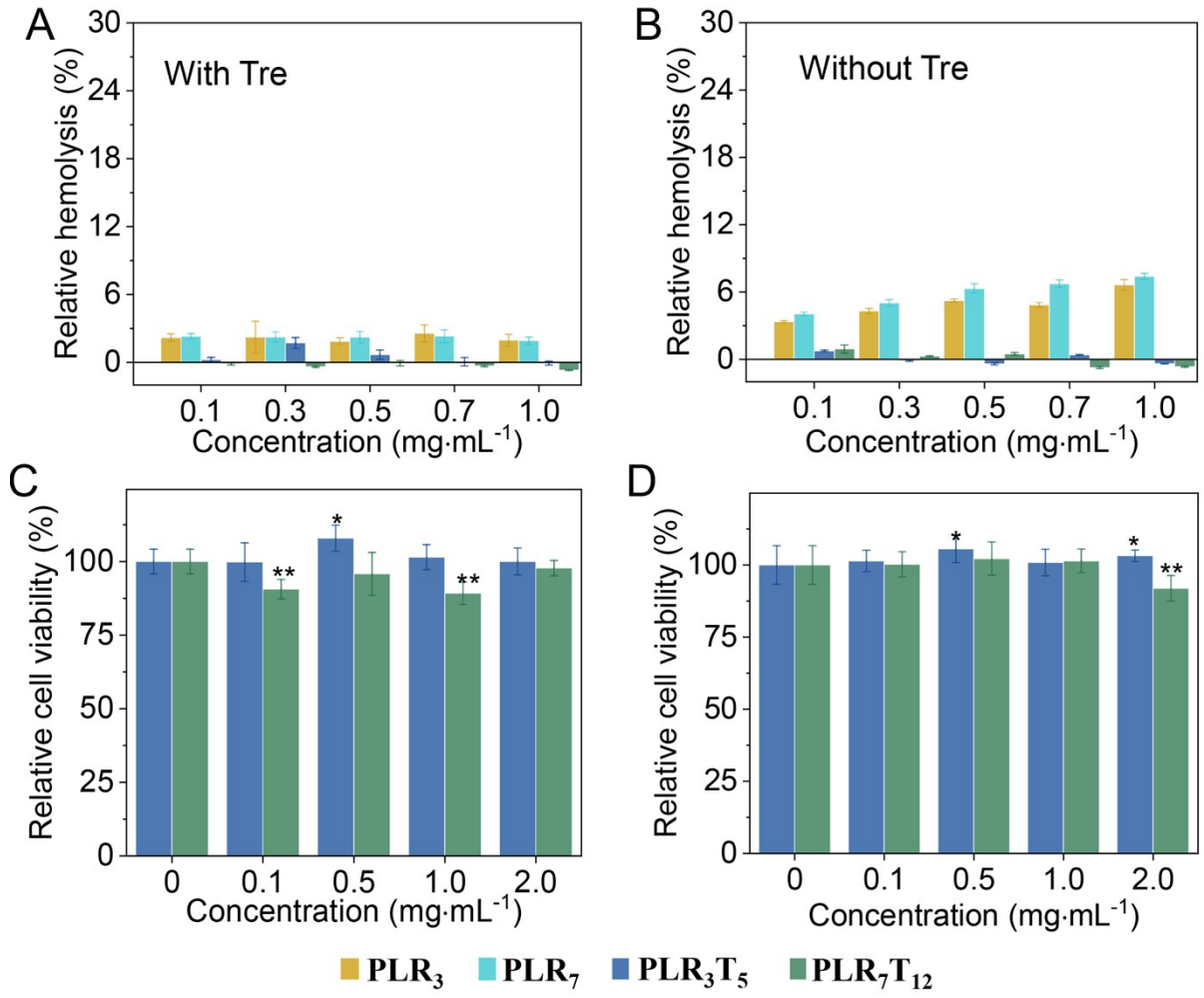

Fig. S8 A,B) Hemolysis of RBCs after incubated with different concentrations of (glyco)peptides at 37 °C and pH 7.4 for 2 h. A) (glyco)peptides with 0.36M **Tre**. B) (glyco)peptides alone. The hemolysis of **PLR$_3$** and **PLR$_7$** was higher than that of **PLR$_3$T$_5$** and **PLR$_7$T$_{12}$** with or without 0.36 M **Tre**, but some agglutinations of RBCs appeared for both **PLR$_3$** and **PLR$_7$**. C,D) Concentration-dependent relative cell viability of different (glyco)peptides at 37 °C and pH 7.4 for 24 h against L929 cells. C) Alamar Blue assay. D) MTT assay. Values are means ± the standard deviation, $^{*}p < 0.05$, $^{**}p < 0.01$, $n = 3$, and all samples were compared with control sample without (glyco)peptides. The L929 cell viability was over 80% in the concentration ranges from 0.1 mg·mL^{-1} to 2.0 mg·mL^{-1} for **PLR$_3$** and **PLR$_7$**, **PLR$_3$T$_5$** and **PLR$_7$T$_{12}$**.

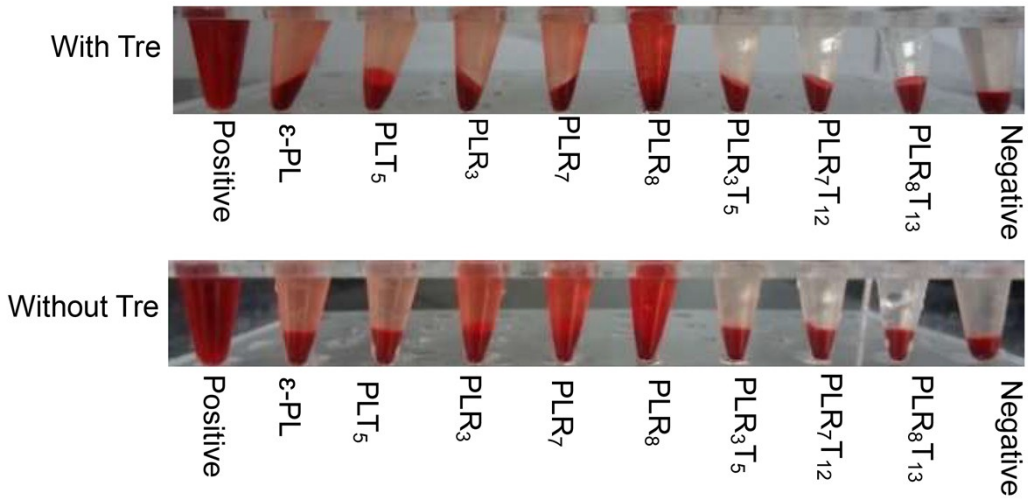

Fig. S9 Digital pictures of samples after incubation with 1 mg·mL^{-1} (glyco)peptides/0.36 M **Tre** and with 1 mg·mL^{-1} (glyco)peptides alone. It could be observed that the samples with **PLR_8T_{13}** exhibited negligible hemolysis, even similar to the negative control.

Dynamic light scattering (DLS) analysis

The zeta potentials were measured using a laser light scattering spectrometer (DLS, Zetasizer Nano Zs90, Malvern, UK).[5] The (glyco)peptide and/or RBCs mixture solutions in the buffer at pH 7.4 were used for the DLS measurement which was performed at an angle of 90º in a 10 mm diameter cell at 25 ºC, and each sample was repeated in triplicate. Glycopeptide solution at 1.0 mg·mL^{-1} was prepared in the buffer at pH 7.4. (Glyco)peptide (1mg·mL^{-1}) was mixed with RBCs (100/1, *v*/*v*).

Fig. S10 also showed that zeta potential values of **PLR$_3$T$_5$**, **PLR$_7$T$_{12}$** and **PLR$_8$T$_{13}$** were lower than those of ε-**PL**, **PLT$_5$** or **PLR$_3$**, **PLR$_7$** and **PLR$_8$**. Furthermore, the zeta potential values of all sample solutions decreased after mixing with RBCs possible due to negative charge existing on the surface of RBC membrane. Interestingly, the zeta potentials of samples with both Arg(Tos) and **Tre** mixing with RBCs were similar with that of control sample with RBCs alone, while the values of samples with Arg(Tos) and **Tre** mixing with RBCs increased. The results indicated that the samples incorporation with both Arg(Tos) and **Tre** has no zeta potential disruption on RBCs.

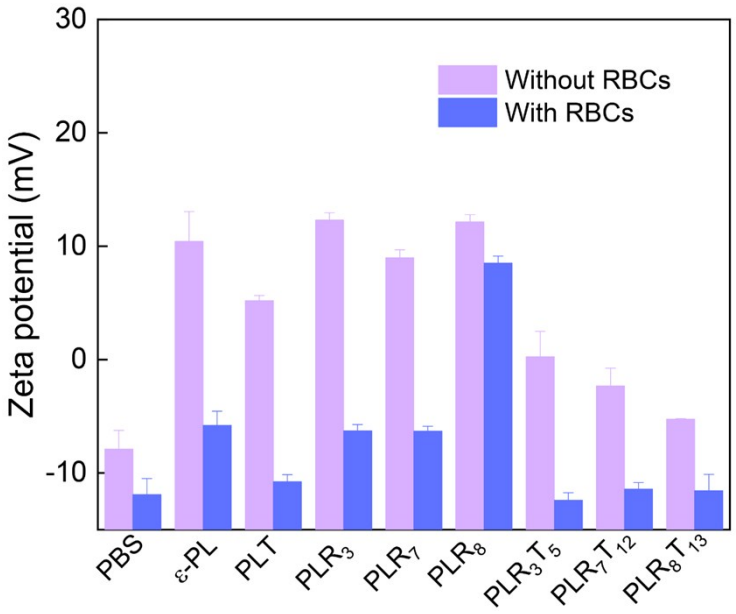

Fig. S10 Zeta potential of (glyco)peptides with RBCs or without RBCs at 1 mg·mL^{-1}.

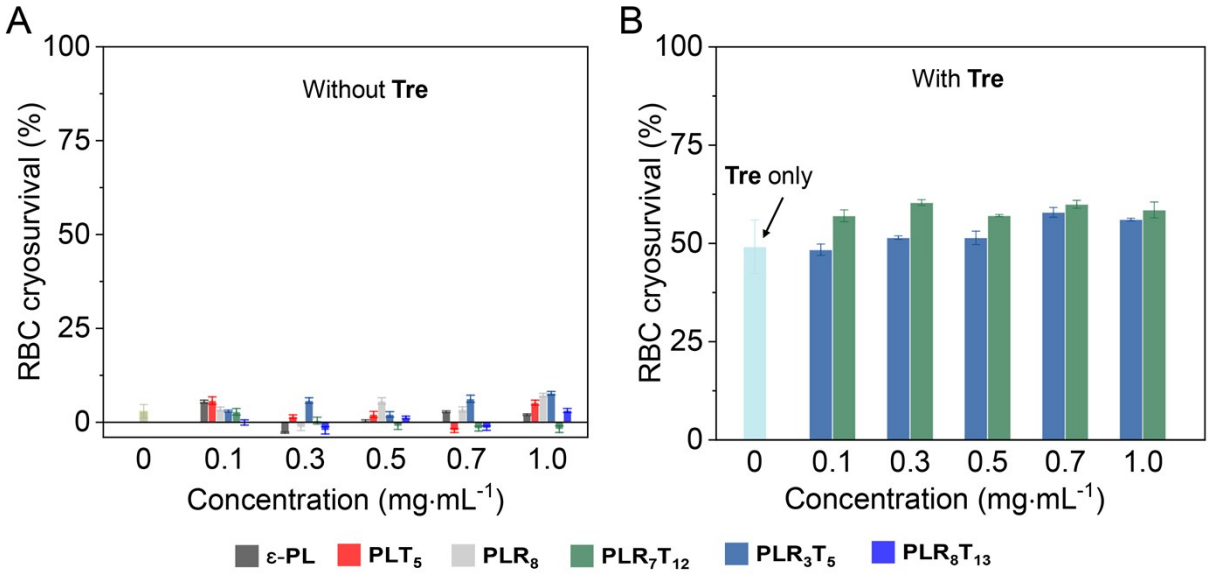

Fig. S11 RBC cryosurvival. A) By using (glyco)peptides alone. B) By using **PLR$_3$T$_5$**/0.36 M **Tre** or **PLR$_7$T$_{12}$** /0.36 M **Tre**. Values are means ± the standard deviation, and all samples were compared with control sample without any (glyco)peptides.

As shown in Fig. S11, the cryopreservation of (glyco)peptides or (glyco)peptide/**Tre** on sheep RBCs was measured. Fig. S11A showed the cryosurvival of RBCs was below 10% when the polymer was used alone. Fig. S11B showed both **PLR$_3$T$_5$** and **PLR$_7$T$_{12}$** combing with 0.36 M **Tre** could improve RBC cryosurvival compared with 0.36 M **Tre** alone. The results suggested that the synthesized (glyco)peptides could not cryoprotect RBCs, but could synergistically improve the RBC cryosurvival with 0.36 M **Tre**.

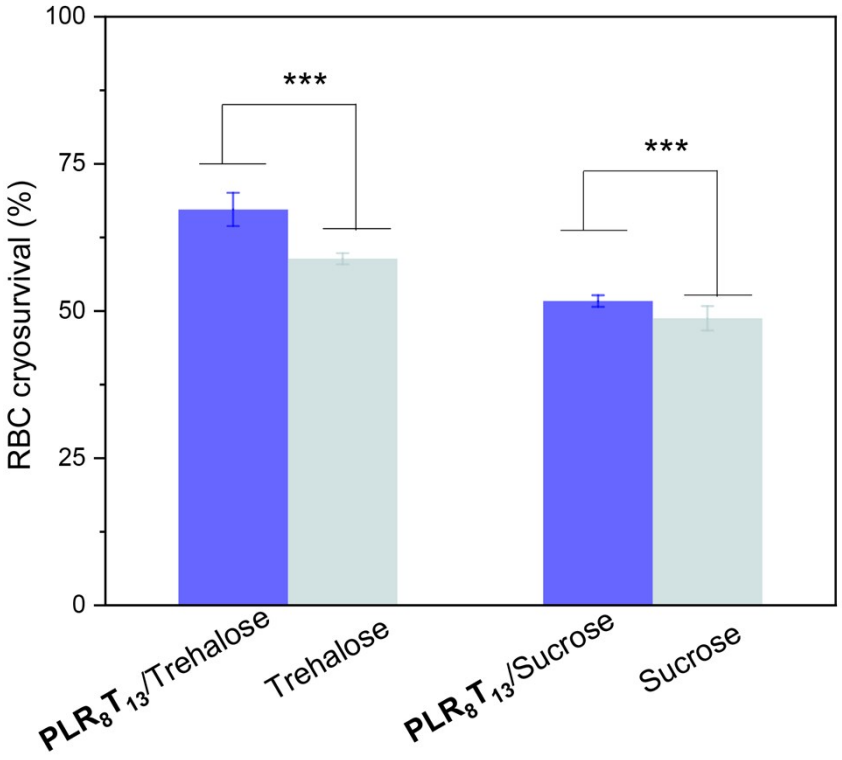

Fig. S12 RBC cryosurvival with **PLR_8T_{13}**/0.36 M trehalose, 0.36 M trehalose, **PLR_8T_{13}**/0.36 M sucrose and 0.36 M sucrose. Values are means ± the standard deviation, $^{***}p < 0.001$, $n = 3$.

As shown in **Fig. S12**, under identical condition, the RBCs cryosurvival of **PLR_8T_{13}**/sucrose sample (51.7±1.0%) was significantly lower than that of **PLR_8T_{13}**/trehalose sample (67.3 ±2.8%). Meanwhile, the RBCs cryosurvival of sucrose was also significantly lower than that of trehalose. The results suggested that trehalose actually performed a special role in cryopreservation of RBCs, and **PLR_8T_{13}** could synergistically improve RBCs cryosurvival with 0.36 M trehalose.

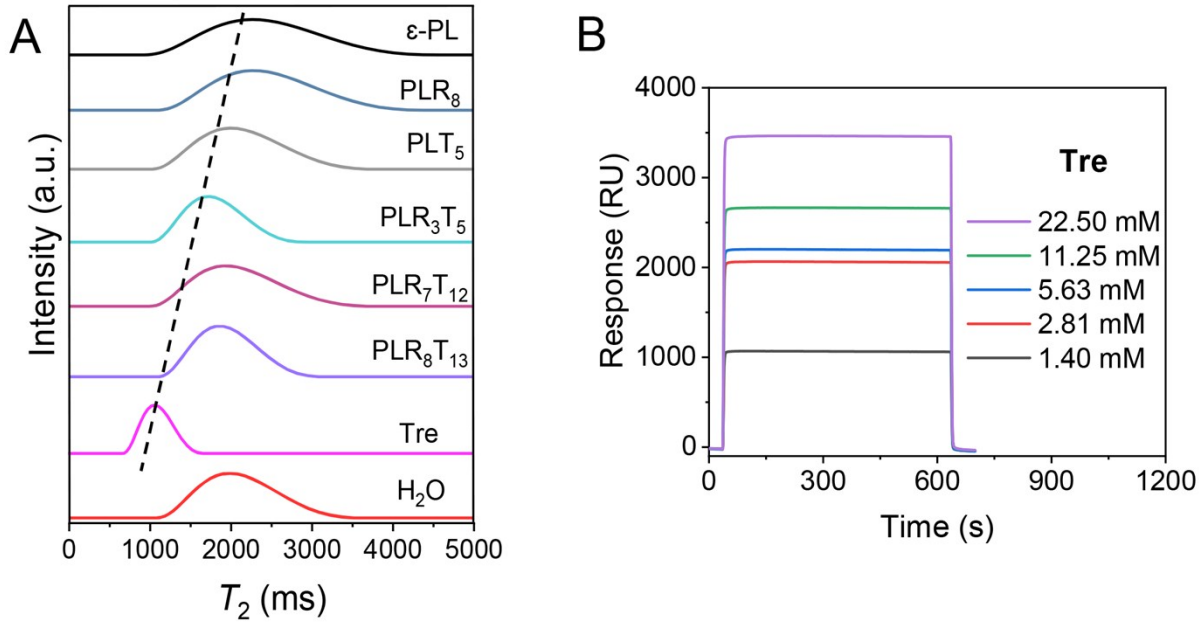

Fig. S13 A) LF NMR relaxation time (T_2) inversion spectra of water in the different (glyco)peptides with 1mg·mL^{-1}. B) SPR sensorgrams for **Tre**.

In Fig. S13A, the spectra peaks of pure (glyco)peptide aqueous solutions showed similar transverse spin-spin relaxation time (T_2) values (Table S2) with that of pure water, and the peaks of **PLR$_3$T$_5$** solution would get narrow and T_2 values would decrease among the samples of ε-**PL**, **PLT$_5$**, **PLR$_8$** and **PLR$_3$T$_5$** solution. However, the peaks of samples of **PLR$_3$T$_5$**, **PLR$_7$T$_{12}$** and **PLR$_8$T$_{13}$** solution were similar with pure water. The results indicated that water molecules moved without being restricted due to weak interactions between (glyco)peptides and water molecules.

It could be found (Fig. S13B) that RU immediately decreased after the end of the addition of the **Tre** solution as a result of quick release of the interacted components, indicating that the interaction between **Tre** and DOPC liposome was weak due to stronger **Tre**-water interaction than Tre-DOPC interaction. In addition, the RU values of **Tre** increased with the concentration of sample solution increasing, suggesting that the interaction between **Tre** and DOPC could be enhanced under higher concentration.

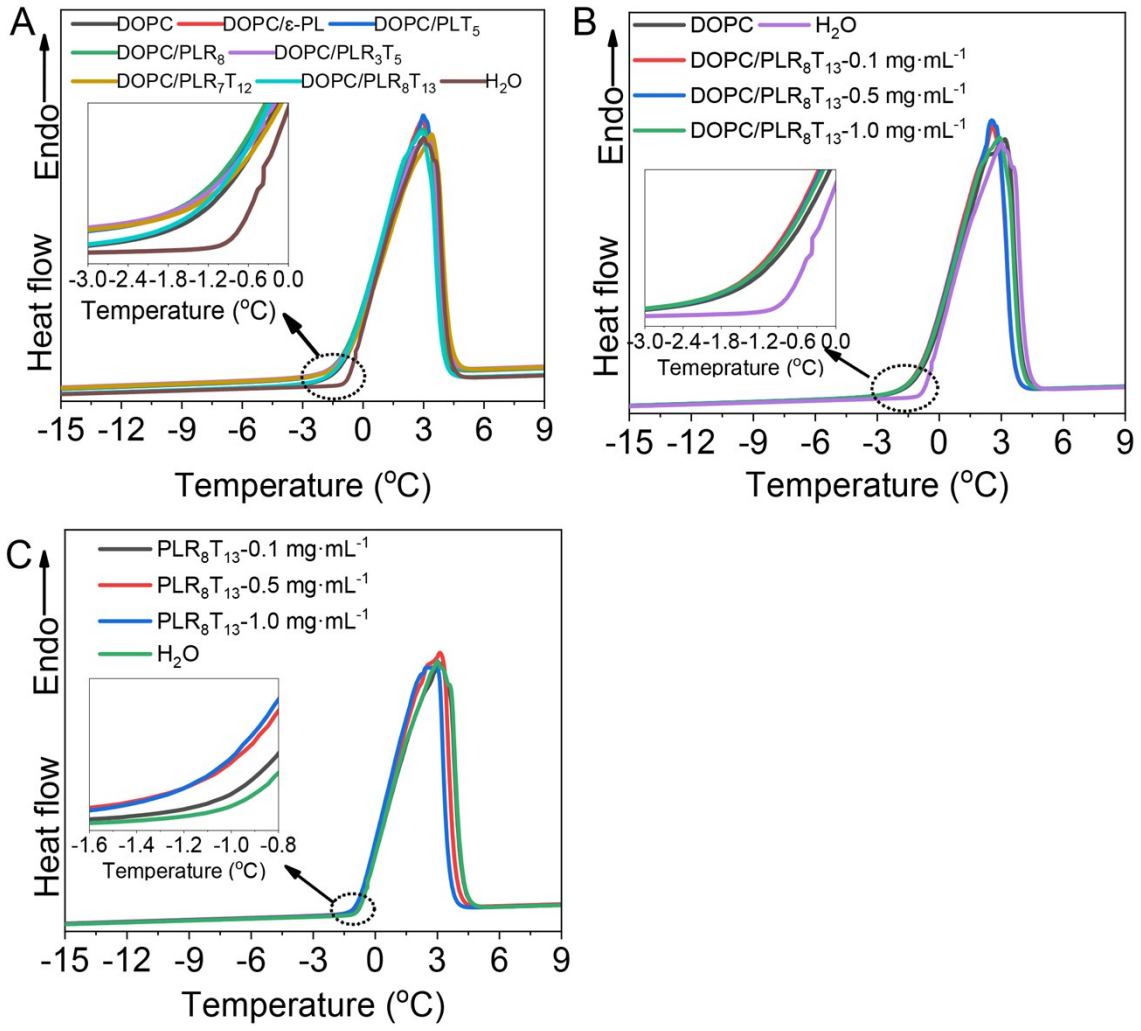

Fig. S14 DSC heating thermograms. A) 1 mM DOPC or 1mg·mL^{-1} (glyco)peptide mixtures. B) 1 mM DOPC with **PLR$_8$T$_{13}$** with different concentration. C) **PLR$_8$T$_{13}$** with different concentration. Scans were obtained at a heating rate of 2 °C·min^{-1}.

Fig. S14A showed the onset temperature (T_{onset}) of ice in ε-**PL**, **PLT$_5$**, **PLR$_8$** and **PLRT**s solutions mixing with DOPC were slightly lower than that of pure water. Compared to pure water, Fig. S14B showed that the T_{onset} of ice in DOPC/**PLR$_8$T$_{13}$** solutions were slightly lower, but Fig. S14C showed the melt points of **PLR$_8$T$_{13}$** solutions negligibly changed.

Table S2 Relaxation time (T_2) of water in the compound mixtures containing 1 mM DOPC, 1mg·mL^{-1} (glyco)peptide or 0.36 M **Tre**.

Compound	T_2 (ms)
DOPC/**PLR_8T_{13}**/**Tre**	1288
DOPC/**PLR_8T_{13}**	1755
DOPC/**Tre**	1390
DOPC	1635
PLR_8T_{13}/**Tre**	1080
Tre	950
ε-PL	2140
PLR_8	2180
PLT_5	1910
PLR_3T_5	1700
PLR_7T_{12}	1890
PLR_8T_{13}	1855
H_2O	1930

Ice recrystallization inhibition (IRI) assay

The IRI measurement was performed by the splat-cooling method as previously reported.[26-28] A 20 μl droplet of sample solution was dropped onto the cover glass precooled to -60 °C from a height of 1.5 m, forming a piece of polycrystalline ice. The temperature was increased to -6 °C at a rate of 25 °C·min^{-1}, and then the samples were annealed at -6 °C for 45 min on the Linkman cooling stage (C194). Photographs were obtained randomly using a Nikon polarized optical microscope (LV 100ND, Japan) equipped with a digital camera (Nikon Y-TV55, Japan). For every sample, three experimental runs were performed, and 5 images were captured for each experimental run. The size of the largest 10 grains of each image was measured using Image J. Among these 150 data for each sample, 100 corresponding to the largest grains were chosen to calculate the mean largest grain size (MLGS). This average value was then compared to that of a PBS buffer negative control.

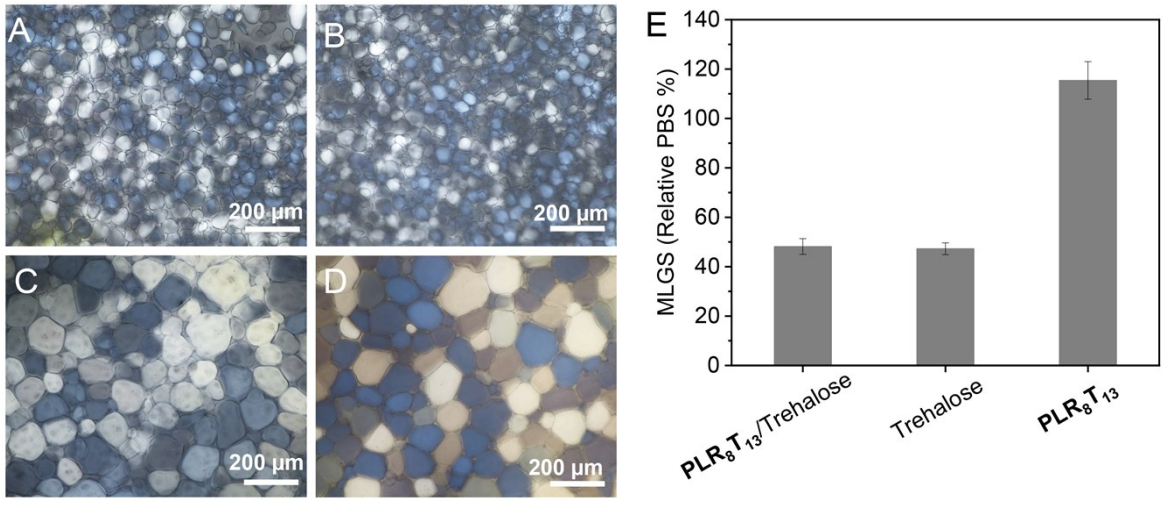

Fig. S15 IRI activity. The polarized optical microscopy images showing native ice crystal growth annealing at -6 °C for 45 min by addition of A) 1 mg·mL^{-1} **PLR_8T_{13}**/0.36 M trehalose, B) 0.36 M trehalose, C) 1 mg·mL^{-1} **PLR_8T_{13}** and D) PBS. E) The mean largest grain sizes (MLGS) obtained from buffer solutions of 1 mg·mL^{-1} **PLR_8T_{13}**/0.36 M trehalose, 1 mg·mL^{-1} **PLR_8T_{13}** and 0.36 trehalose relative to PBS solution alone. Error bars represent the STDEV of the size of 100 ice crystals.

Fig. S15 showed ice recrystallization inhibition activity of **PLR_8T_{13}** or **Tre**. In terms of **PLR_8T_{13}**/**Tre** and **Tre**, the MLGS of ice crystal was almost similar (about 47%), while that for **PLR_8T_{13}** addition alone was the largest (about 116%). The results indicated that **PLR_8T_{13}** has no IRI activity, but **PLR_8T_{13}** could protect cells from osmatic injury by membrane stabilization.

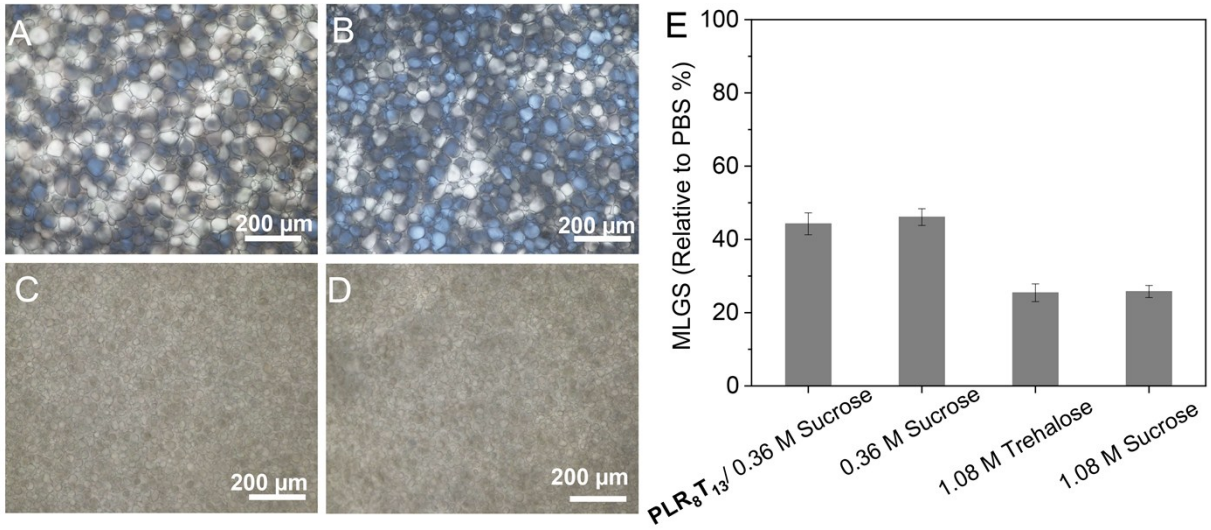

Fig. S16 IRI activity. The polarized optical microscopy images showing native ice crystal growth annealing at -6 ℃ for 45 min by addition of A) 1 mg·mL^{-1} **PLR_8T_{13}**/0.36 M sucrose, B) 0.36 M sucrose, C) 1.08 M trehalose and D) 1.08 M sucrose. E) The mean largest grain sizes (MLGS) obtained from buffer solutions of 1 mg·mL^{-1} **PLR_8T_{13}**/0.36 M sucrose, 1.08 M trehalose and 1.08 M sucrose relative to PBS solution alone. Error bars represent the STDEV of the size of 100 ice crystals.

Fig. S16 showed the IRI activity of **PLR_8T_{13}** or sucrose. It could be observed that both **PLR_8T_{13}**/sucrose and sucrose showed IRI activity, and the size of ice crystal could be inhibited when the concentration was increased.

References

1. K. Debnath, N. Pradhan, B. K. Singh, N. R. Jana and N. R. Jana, *ACS Appl. Mater. Interfaces*, 2017, **9**, 24126-24139.
2. H. Fang, Z. Guo, L. Lin, J. Chen, P. Sun, J. Wu, C. Xu, H. Tian and X. Chen, *J. Am. Chem. Soc.*, 2018, **140**, 11992-12000.
3. M. Stefanic, K. Ward, H. Tawfik, R. Seemann, V. Baulin, Y. Guo, J. B. Fleury and C. Drouet, *Biomaterials*, 2017, **140**, 138-149.
4. Q. Q. Guo, Y. Zhao, X. M. Dai, T. Zhang, Y. Yu, X. Zhang and C. Li, *ACS Appl. Mater. Interfaces*, 2017, **9**, 16834-16847.
5. B. Liu, Q. Zhang, F. Zhou, L. Ren, Y. Zhao and X. Yuan, *ACS Appl. Mater. Interfaces*, 2019, **11**, 14538-14547.
6. B. Liu, T. Yao, L. Ren, Y. Zhao and X. Yuan, *Colloids Surf. B Biointerfaces*, 2018, **172**, 330-337.
7. C. Li, S. Bai, X. Li, Y. Zhao, L. Ren, K. Zhu and X. Yuan, *ACS omega*, 2018, **3**, 7371-7379.
8. S. Bai, X. Li, R. Zhang, C. Li, K. Zhu, P. Sun, Y. Zhao, L. Ren and X. Yuan, *Chem. Eng. J.*, 2019, **357**, 667-677.
9. R. Zhang, S. Yu, S. Chen, Q. Wu, T. Chen, P. Sun, B. Li and D. Ding, *J. Phys. Chem. B*, 2014, **118**, 1126-1137.
10. E. M. Erb, X. Chen, S. Allen, C. J. Roberts, S. J. Tendler, M. C. Davies and S. Forsen, *Anal. Biochem.*, 2000, **280**, 29-35.
11. H. Moriwaki, K. Yamada and H. Nakanishi, *J. Agric. Food. Chem.*, 2017, **65**, 5390-5396.
12. T. H. Lee, D. J. Hirst, K. Kulkarni, M. P. Del Borgo and M. I. Aguilar, *Chem. Rev.*, 2018, **118**, 5392-5487.
13. J. G. G. Luz, D. E. P. Souto, G. F. Machado-Assis, M. de Lana, L. T. Kubota, R. C. S.

Luz, F. S. Damos and H. R. Martins, *Sens. Actuators B: Chem.*, 2015, **212**, 287-296.
14. J. Yang, C. Pan, J. Zhang, X. Sui, Y. Zhu, C. Wen and L. Zhang, *ACS Appl. Mater. Interfaces*, 2017, **9**, 42516-42524.
15. S. Lee, J. H. Lee, H. W. Kim and J. W. Hong, *Cryobiology*, 2018, **85**, 33-38.
16. J. R. Colina, M. Suwalsky, M. Manrique-Moreno, K. Petit, L. F. Aguilar, M. Jemiola-Rzeminska and K. Strzalka, *Colloids Surf. B Biointerfaces*, 2019, **173**, 742-750.
17. R. C. Deller, M. Vatish, D. A. Mitchell and M. I. Gibson, *Nat. Commun.*, 2014, **5**, 3244.
18. G. Yu, R. Li and A. Hubel, *Langmuir*, 2019, **35**, 7388-7395.
19. A. L. Lynch, R. J. Chen, P. J. Dominowski, E. Y. Shalaev, R. J. J. Yancey and N. K. H. Slater, *Biomaterials*, 2010, **31**, 6096-6103.
20. C. Qi, R. Zhang, K. Jia, Y. Lei and W. Wu, *J. Mol. Liq.*, 2016, **224**, 1233-1241.
21. R. Zhang, W. Zeng, X. Meng, J. Huang and W. Wu, *Chem. Phys.*, 2012, **402**, 130-135.
22. W. K. Surewicz, H. H. Mantsch and D. Chapman, *Biochemistry*, 1993, **32**, 389-394.
23. G. Ghosh, R. Barman, J. Sarkar and S. Ghosh, *J. Phys. Chem. B*, 2019, **123**, 5909-5915.
24. J. Freudenberg and W. H. Binder, *Macromolecules*, 2019, **52**, 4534-4544.
25. T. J. Anchordoguy, A. S. Rudolph, J. F. Carpenter and J. H. Crowe., *Cryobiology* 1987, **24**, 324-331.
26. S. Wu, C. Zhu, Z. He, H. Xue, Q. Fan, Y. Song, J. S. Francisco, X. C. Zeng and J. Wang, *Nature communications*, 2017, **8**, 15154.
27. M. Hasan, A. E. R. Fayter and M. I. Gibson, *Biomacromolecules*, 2018, **19**, 3371-3376.
28. B. Graham, A. E. R. Fayter, J. E. Houston, R. C. Evans and M. I. Gibson, *J. Am. Chem. Soc.*, 2018, **140**, 5682-5685.